Zero : Jurnal Sains, Matematika, dan Terapan
E-ISSN : 2580-5754; P-ISSN : 2580-569X
Volume 10, Number 2, 2026
DOI: 10.30829/zero.v10i2.29945
Page: 719-730

Hydraulic Diagnosis of Urban Flood Mechanisms using HEC-RAS: A Case Study of the Bontang River, Indonesia

[1]Viva Oktaviani
Department of Civil Engineering, University of 17 August 1945 Samarinda, Indonesia

[2]Heri Purnomo
Department of Civil Engineering, University of 17 August 1945 Samarinda, Indonesia

Article Info

Article history:

Accepted: 10 July 2026

Keywords:

HEC-RAS;
Nakayasu SUH;
Retention pond;
Sluice gate backwater;
Urban drainage.

ABSTRACT

Flooding along the Bontang River in Gunung Telihan Village, Bontang City, recurs almost annually, yet its causes had not been diagnosed mechanistically. This study applied one dimensional steady-flow HEC-RAS 4.1 modeling to a 1,936 m reach, using primary topographic data and design discharges (Q2, Q10, Q20) from the Nakayasu Synthetic Unit Hydrograph. Unlike prior single mechanism studies, the analysis resolved four co occurring flood mechanisms: bank-asymmetry overflow, right bank levee overflow, undersized sluice-gate backwater, and a downstream constriction. Although nominal channel capacity (13.83 m3/s) marginally exceeded Q2 (11.88 m3/s), the low right bank reduced the effective overflow threshold below Q2. A 95% confidence interval on design discharge, computed using Kite's asymptotic method, indicated the downstream constriction could approach overflow at the upper bound of Q10 uncertainty. An independent tidal sensitivity check showed the tidal range effect at the confluence (2.2 m) exceeded the sluice-gate backwater step alone (0.42-0.68 m). A planned condition simulation combining retention ponds, levee reinforcement, and gate augmentation achieved safe status at all critical points, indicating site differentiated intervention is a promising, land feasible direction pending detailed design verification.

Corresponding Author:

Viva Oktaviani,
Department of Civil Engineering,
University of 17 August 1945 Samarinda, East Kalimantan, Indonesia
Email: viva@untag-smd.ac.id

1. INTRODUCTION

Urban flood management remains a persistent challenge in rapidly developing Indonesian coastal cities, where intensifying inundation is driven by catchment imperviousness, riparian encroachment, and constrained channel conveyance [1]. River hydraulic modeling is now an essential planning instrument, particularly for diagnosing multiple co occurring inundation mechanisms that qualitative field assessment cannot resolve [2], [3]. HEC-RAS is widely adopted for this purpose, with documented applications in inundation mapping and the evaluation of structural interventions [4], [5], [6].

Bontang City, an industrial coastal city in East Kalimantan, presents a distinctive setting: its lower drainage is tidally influenced by the Makassar Strait, while rapid riparian encroachment constrains conventional channel widening. Field reconnaissance within the Bontang Urban Drainage System (Block BG.05) identified four recurring inundation sites along the Gunung Telihan reach: upstream of Taman Husada Regional Hospital, the Jalan Bandung residential corridor, the sluice gate at the river confluence, and the constriction near Al Jihad Mosque.

HEC-RAS is well established for urban flood diagnosis and mitigation evaluation [4], [5], [7], [6], [8], and recent regional studies have addressed channel overflow [2], tidal backwater [9], [10], and compound-flood/inundation mapping, including for the new East Kalimantan capital region [11], [12], [13], [14], [15], [16], [17],[18]. However, each of these studies resolves a single dominant mechanism per reach. This single process framing does not transfer to a small tidal urban river such as the Bontang, where channel undersizing, bank asymmetry, confluence gate backwater, and a downstream constriction operate simultaneously along one 1,936-m reach. Diagnosing such co occurring mechanisms, and linking each to a distinct rehabilitation measure, is the gap this study addresses, and is, to the authors' knowledge, not yet reported for coastal urban rivers of East Kalimantan.

Accordingly, this study aims to: (1) develop a 1D steady flow HEC-RAS 4.1 model from primary topographic data; (2) simulate flood water surface profiles for the 2-, 10-, and 20-year return periods; (3) diagnose the flood mechanism at each critical point; (4) quantify the channel capacity deficit; and (5) evaluate proposed mitigation through planned condition simulation. The design discharges driving this model were derived using the Nakayasu Synthetic Unit Hydrograph, an approach previously coupled with HEC HMS and HEC-RAS for flood hydrograph analysis in comparable ungauged catchments [19]. The research logic is summarized in Figure 1.

This study is explicitly scoped as a steady flow diagnostic assessment rather than a predictive or design grade hydraulic model, appropriate to a data constrained, ungauged system at the mechanism identification stage. Unsteady tidal coupling simulation, while valuable for refining inundation magnitude, falls outside this diagnostic scope and is identified as the natural next phase of this research program (Section 4); an interim, non unsteady quantitative check on tidal sensitivity is presented in Section 3.7.

Figure 1. Conceptual framework linking data inputs (topographic survey, Nakayasu SUH discharges) through HEC-RAS modeling to flood mechanism diagnosis and site differentiated rehabilitation strategy.
Source: Authors, 2025.

2. RESEARCH METHOD

2.1 Study Area and Topographic Survey

This study employed a computational hydraulic modeling design using one dimensional steady flow analysis in HEC-RAS 4.1, applied to a data constrained, ungauged urban river system. The approach was selected as appropriate for the mechanism diagnosis stage of flood risk assessment, consistent with comparable practice for ungauged urban rivers [20],[21]. The study reach encompasses 1,936 meters of the Bontang River from STA 0+000 to STA 1+936, within Gunung Telihan Village, Bontang City, East Kalimantan Province (Figures 2-3). All primary field data, topographic survey, rainfall records, and hydraulic structure geometry, originate from a self managed (swakelola) flood control planning project executed by PENATEK 45, Universitas 17 Agustus 1945 Samarinda, for the Bontang City Public Works and Spatial Planning Agency (PUPR) [22]; subsequent references to this source are cited as [22].

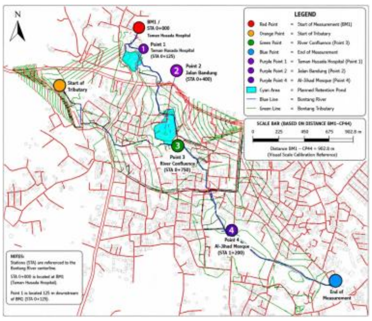

Figure 2. Study Area Location Map, Bontang River, Gunung Telihan Village, showing the survey benchmark (BM1, STA 0+000) and four flood observation points (Point 1-4, STA 0+125 to 1+200) along the modeled 1,936 m reach. Source: Topographic Survey Report, PENATEK 45 (2025), Bab IV, Gambar 4.2[23], with observation point annotations and scale calibration added by the authors.

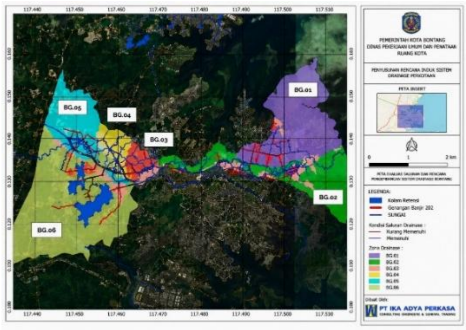

Figure 3. Bontang Urban Drainage System Master Plan showing Block BG.05 (study area) among six drainage zones (BG.01-BG.06). Source: Rencana Induk Sistem Drainase Perkotaan Kota Bontang, Dinas Pekerjaan Umum dan Penataan Ruang Kota Bontang, prepared by PT Ika Adya Perkasa Consulting Engineers & General Trading [22].

2.2 Data Source and Variables

Primary topographic data were collected using a closed traverse polygon as the horizontal control framework, measured with Theodolite (Wild T0 and Wild T2) instruments and referenced to permanent Bench Marks (20 x 20 x 100 cm). Differential leveling using a calibrated automatic level (Wild/Zeiss Ni2) provided elevation data. A total of 19 cross sections were measured at 50-meter intervals along the main reach, reduced to 25-meter intervals at channel bends, with each cross-section extending at least 20 meters beyond each bank.

Design flood discharges were derived from 10 years of daily maximum rainfall data (2015-2024) from Stasiun Kanaan. The absence of continuous streamflow gauging precluded formal hydrologic and hydraulic calibration (Nash Sutcliffe efficiency, RMSE, or equivalent), and is the reason the validation strategy in Section 3.4 relies on plausibility and spatial consistency checks rather than a statistical goodness of fit metric.

Data Availability Statement. The primary topographic survey, rainfall records, and hydraulic structure geometry used in this study originate from an unpublished technical report [22] produced under a self managed project by PENATEK 45, with publication permission granted covering the report's data, tables, and site plan drawings. This permission does not extend to the original HEC-RAS software project files (geometry and plan files), which could not be recovered for this submission (Section 3.5).

Reproducibility Statement. Despite repeated attempts to contact the technical staff who executed the original HEC-RAS runs, the original geometry and plan files (.g0x/.f0x) could not be recovered. As mitigation, all machine-readable parameters from the source technical report [22] are provided in full in Tables 4-7, together with the network schematization in Section 2.5. Two quantities, bank heights at Points 1-2 (Table 5 note) and the Pond 1 sub catchment delineation (Section 3.5), could not be independently re verified; neither affects the core four-mechanism diagnosis, which rests on the independently verified geometry in Table 5 and the simulation outputs in Tables 8-10. Two additional independent documentary sources strengthen the reproducibility basis: a separate topographic survey report [23], which confirms the field survey methodology and provided the basemap for Figure 2 with precise UTM Zone 50N benchmark coordinates; and the official Bontang Urban Drainage System Master Plan [22], used directly as the basis for Figure 3.

2.3 Rainfall Frequency Distribution Sensitivity

Four candidate distributions, Gumbel Type I, Log Normal 2 Parameter, Log Pearson Type III, and Frechet (Gumbel Type II), were evaluated using Chi Square and Smirnov Kolmogorov goodness of fit tests at α = 5% (Table 1), consistent with standard practice for statistical distribution testing in short-record rainfall frequency analysis[24], [25].

Table 1. Goodness-of-fit test results for frequency distributions (n = 10, α = 5%, DK = 2)

Distribution method	Dmax (S-K)	Dcrit (S-K)	S-K result	χ^2 calc	χ^2 crit	DK	Status
Gumbel Type I	0.1233	0.4090	Pass	3.000	5.991	2	Selected
Log Pearson Type III	0.3448	0.4090	Pass	3.000	5.991	2	Pass
Log Normal 2-Param.	0.1344 *	0.4090	Pass	5.000	5.991	2	Pass
Frechet (Gumbel II)	0.1066 **	0.4090	Pass	3.000	5.991	2	Pass

Source: PENATEK 45 (2025) [22], with corrections detailed below.

*The Log-Normal 2 Parameter Dmax value originally reported exceeded the theoretical upper bound of the Smirnov Kolmogorov statistic [0,1], traced to an incorrect cumulative probability formula in the source spreadsheet. The corrected calculation, applying the standard normal CDF $\Phi(K)$, yields Dmax = 0.1344, reversing the originally reported rejection.

**Similarly, the Frechet Dmax value originally reported (0.8392) was traced to a spreadsheet labeling error duplicating the Log-Pearson Type III results. The corrected calculation yields Dmax = 0.1066.

With both corrections applied, all four candidate distributions pass the Smirnov Kolmogorov test. Gumbel Type I is retained as the primary design distribution on combined grounds: (i) the Dmax margin between Gumbel I and Frechet (0.0167) is small and not materially decisive; (ii) Gumbel Type I is the distribution most widely recommended for short record daily rainfall frequency analysis in Indonesian practice, consistent with SNI 2415:2016 [26]; and (iii) the multi distribution sensitivity screening (Table 3) shows the choice does not materially affect diagnostic conclusions.

Table 2. Design rainfall (Gumbel Type I method)

Return period (years)	Design rainfall (mm)
2	95.18
10	148.38
20	168.71

Data source: 10 years of daily maximum rainfall records (2015-2024), Stasiun Kanaan, PENATEK 45 (2025)[22].

Table 3. Distribution sensitivity comparison of peak discharge across all modeled sub catchments (m^3/s)

Sub-catchment	T (yr)	Gumbel I	Log-Normal 2P	LP III	Frechet	Range (%)
Bontang-1 (0+000-0+750)	2	11.88	11.86	11.63	11.48	-3.4 to -0.2
Bontang-1	10	18.52	16.68	16.82	16.74	-10.0 to -9.1
Bontang-1	20	21.06	18.45	19.23	19.33	-12.4 to -8.2
Bontang-1	100	26.80	22.52	24.50	26.77	-16.0 to -0.1
Tributary	2	2.46	2.46	2.41	2.37	-3.7 to 0.0
Tributary	10	3.83	3.45	3.48	3.46	-10.1 to -9.1
Tributary	20	4.35	3.81	3.97	3.99	-12.4 to -8.3
Tributary	100	5.54	4.65	5.06	5.53	-16.1 to -0.2
Bontang-2 (0+750-1+936)	2	4.77	4.76	4.67	4.61	-3.4 to -0.2
Bontang-2	10	7.44	6.70	6.76	6.72	-10.0 to -9.1
Bontang-2	20	8.46	7.41	7.72	7.77	-12.4 to -8.2
Bontang-2	100	10.77	9.05	9.84	10.76	-16.0 to -0.1

Source: derived by linear scaling of Nakayasu SUH results (Gumbel I basis; source technical report[22]) using design rainfall ratios.

To formalize discharge uncertainty from the short 10 year record, 95% confidence intervals for Q10 and Q20 were computed using Kite's (1977) asymptotic standard error formula for Gumbel quantiles [27]:

$$SE(X_T) = \frac{S_d}{\sqrt{n}}\sqrt{1 + 1.1396K_T + 1.1K_T^2} \quad (1)$$

with n = 10 and Sd = 26.8197. This analytical approach was adopted in place of numerical bootstrap resampling, providing an equivalent, standard, and independently reproducible estimate of sampling uncertainty, consistent with WMO guidance [28]. Full results are presented in Table 13 (Section 3.7).

2.4 Analytical Methods and Equations

One-dimensional steady flow modeling in HEC-RAS solves the standard energy equation between successive cross sections [4]. Energy losses are computed using the Manning Strickler equation:

$$Q = \frac{1}{n} \cdot A \cdot R^{2/3} \cdot S^{1/2} \quad (2)$$

For sluice gate modeling at the river confluence (Point 3), the backwater profile was computed using the momentum equation, and gate capacity was independently cross checked using the submerged orifice equation:

$$Q = C_d \cdot A \cdot \sqrt{2gH} \quad (3)$$

with discharge coefficient Cd = 0.60, gate opening area A = 0.283 m^2, and effective head H ≈ 1.1-2.6 m.

2.5 HEC-RAS Model Configuration

The model was schematized as a two-reach network: Reach Bontang 1 (STA 0+000 to 0+750, 750 m) and Reach Bontang 2 (STA 0+750 to 1+936, 1,186 m), connected at a junction node at STA 0+750, with a separate tributary reach (Anak Sungai Bontang) joining at the confluence. The sluice gate at Point 3 was represented as an Inline Structure (Figure 4).

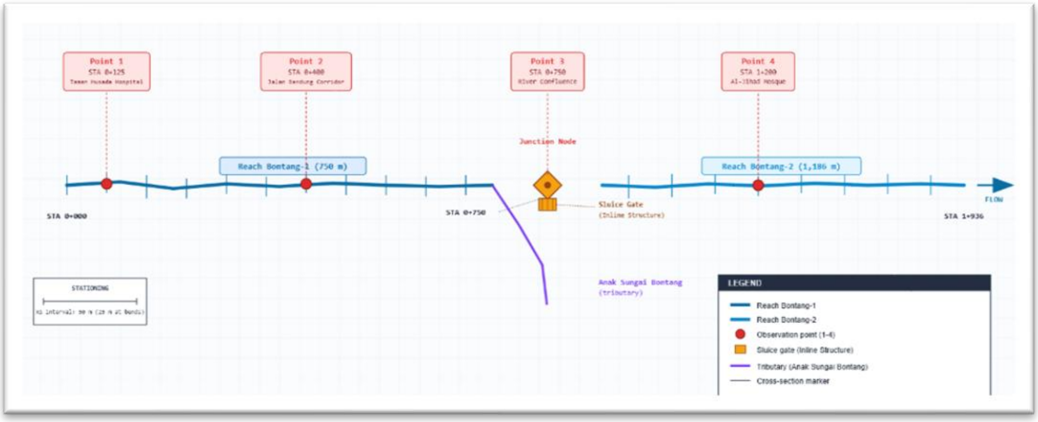

Figure 4. HEC-RAS Two Reach Geometric Schematic of the Bontang River Network. Reconstructed from HEC-RAS configuration described in Section 2.5, based on field-surveyed stationing (PENATEK 45, 2025[22]); styled to resemble the HEC-RAS Geometric Data Editor schematic view, not a direct software export.

Manning's n was assigned by reach: n = 0.025 (Reach Bontang 1), n = 0.028 (Reach Bontang 2), n = 0.030 locally at Point 4, with a ±0.005 sensitivity test confirming the diagnostic conclusions are insensitive to residual roughness uncertainty. Solution tolerances follow HEC-RAS 4.1 defaults (0.01 ft convergence, 20 iterations maximum), as no evidence in the source report [22] indicates these were manually modified. A sensitivity checks on the gate discharge coefficient, varied from 0.60 to the upper bound of the standard range (0.70) [4], increases computed gate capacity from 0.83-1.28 m³/s to 0.97-1.49 m³/s, remaining well below Q2 (11.88 m³/s).

Table 4. HEC-RAS Structural and Hydraulic Parameters

Parameter	Value / Assumption	Basis
Velocity distribution coefficient (α)	1.00 (uniform)	HEC-RAS default [4]
Expansion coefficient (C)	0.1 (gradual) / 0.3 (abrupt, at structure)	HEC-RAS default [4]
Sluice gate structure type	Inline Structure, submerged orifice	Section 2.5
Gate opening geometry	Circular, diameter 0.60 m; A = 0.283 m²	Field surveyed [22]
Discharge coefficient (Cd)	0.60 (range 0.60-0.70)	Standard value [4]
Downstream boundary energy slope	S ≈ 0.0008	Normal depth

Source: parameters confirmed from field survey and structure records [22] where noted; unmarked values follow HEC-RAS default modeling practice[4].

2.6 Software and Tools

Hydraulic simulation was performed using HEC-RAS version 4.1 (US Army Corps of Engineers, Hydrologic Engineering Center). Manning Strickler channel capacity calculations, Nakayasu Synthetic Unit Hydrograph derivation, frequency distribution analysis, and the Kite's asymptotic confidence interval computation were performed using standard spreadsheet based hydrological calculation procedures, following methods documented in the cited technical references.

2.7 Ethical Considerations

This study did not involve human or animal subjects. All primary field data were collected under an institutional self managed (swakelola) project executed by PENATEK 45 for the Bontang City Public Works and Spatial Planning Agency, with formal data use permission granted for academic publication.

3. RESULTS AND ANALYSIS

3.1 Existing Channel Geometry

Topographic survey of the 19 cross sections revealed significant geometric variability, particularly in bottom width and bank heights, reflecting the unregulated natural channel morphology (Table 5).

Table 5. Mean Channel Geometry of Bontang River Based on Cross Section Survey

Parameter	Reach 0+000-0+750	Reach 0+750-1+936	Point 3	Point 4	Unit
Average Bottom Width (b)	4.25	4.80	5.50	4.00	m
Average Depth (h)	1.20	1.10	1.30	1.20	m
Side Slope (m:1)	0.50	0.50	0.50	0.25	H:V
Channel Slope (S)	0.0022	0.0008	0.0015	0.0018	m/m
Manning's n	0.025	0.028	0.025	0.030	-

Left Bank Height (Ht-L)*	1.50	2.00	1.80	1.40	m
Right Bank Height (Ht-R)*	0.70	1.90	1.80	1.40	m

Source: Field topographic survey, PENATEK 45 (2025) [22].

*Bank height values at Point 1 and 2 originate from the original HEC-RAS geometry file, which could not be independently recovered (Section 2.2). Two independent lines of qualitative evidence support the reported asymmetry: (i) the source report documents a low right bank levee at Point 2 as the cause of overflow[22]; and (ii) simulated overflow under Q2 at both points is consistent with field documented flood recurrence.

A critical geometric asymmetry is evident in Reach STA 0+000-0+750: the right bank height (0.70 m) is markedly lower than the left bank (1.50 m), functioning as a broad crested weir directing excess discharge toward the Jalan Bandung residential area.

3.2 Existing Channel Conveyance Capacity

Manning Strickler calculations were performed for all three modeled segments, Reach Bontang 1, the tributary, and Reach Bontang 2, to establish the full channel capacity profile along the system, as summarized in Table 6.

Table 6. Maximum Channel Conveyance Capacity by Segment

Segment	Slope (S)	Mean depth (m)	Mean width (m)	Capacity (m^3/s)	Status
Reach Bontang-1 (0+000-0+750)	0.0022	2.00	4.25	13.83	Marginal at Q2
Anak Sungai Bontang (tributary)	0.0013	2.00	2.20	5.48	Exceeded at Q10
Reach Bontang-2 (0+750-1+936)	0.0008	2.00	4.25	11.97	Exceeded at Q10

Source: Calculation results, 2025 (n = 0.025 uniformly applied); PENATEK 45 [22].

To provide a more granular basis for independent verification than the single mean depth capacity value in Table 6, a stepped conveyance rating curve was constructed for each segment across a range of operating depths, as presented in Table 7.

Table 7. Stepped Conveyance Rating Curve by Segment (n = 0.025 uniform)

Segment	h (m)	b (m)	A (m^2)	P (m)	R (m)	V (m/s)	Q (m^3/s)
Reach Bontang-1	1.00	4.00	4.50	6.24	0.72	1.51	6.79
Reach Bontang-1	1.50	5.00	8.63	8.35	1.03	1.92	16.53
Reach Bontang-1	2.00	6.00	14.00	10.47	1.34	2.28	31.88
Tributary	0.80	0.80	0.96	2.59	0.37	0.74	0.72
Tributary	1.50	2.00	4.13	5.35	0.77	1.21	5.00
Tributary	2.00	4.00	10.00	8.47	1.18	1.61	16.11
Reach Bontang-2	2.00	4.00	10.00	8.47	1.18	1.26	12.64
Reach Bontang-2	2.00	5.00	12.00	9.47	1.27	1.33	15.90
Reach Bontang-2	2.00	6.00	14.00	10.47	1.34	1.37	19.22

Source: Manning Strickler calculations, PENATEK 45 (2025)[22].

At the reference operating depth, Reach Bontang 1 capacity was approximately 13.83 m^3/s. While this exceeds Q2 (11.88 m^3/s), the critical limitation is the asymmetric bank height: the right bank at only 0.70 m sets an effective overflow threshold of about 6.79 m^3/s, below Q2, explaining why flooding recurs with nearly every significant rainfall event.

3.3 HEC-RAS Simulation Results

Steady flow HEC-RAS simulation was performed for all three design discharges (Q2, Q10, Q20) at the four observation points, revealing overflow or backwater conditions beginning from the 2 year return period, as summarized in Table 8.

Table 8. Flood Safety Status at Four Observation Points Based on HEC-RAS Simulation

No	Observation Point	Q2 (11.88 m^3/s)	Q10 (18.52 m^3/s)	Q20 (21.06 m^3/s)
1	Upstream Taman Husada Hospital	Flood	Flood	Flood
2	Jalan Bandung (low levee)	Flood	Flood	Flood
3	River Confluence (sluice gate)	Backwater	Backwater	Backwater
4	Constriction at Al-Jihad Mosque	Safe	Safe	Potential

Source: HEC-RAS simulation results, authors, 2025.

The simulated water surface elevations underlying the flood status classification in Table 8 are reported in full, together with the corresponding bank crown elevations at each observation point, in Table 9.

Table 9. Simulated Water Surface Elevations (WSE) at Observation Points

No	Observation Point	Bank Elev. (m asl)	WSE Q2 (m asl)	WSE Q10 (m asl)	WSE Q20 (m asl)	Status (Q2)
1	Upstream Taman Husada (STA 0+125)	14.87 (R)	15.23	15.65	15.82	OVERFLOW
2	Jalan Bandung (STA 0+400)	14.63 (R)	14.71	14.94	15.05	OVERFLOW
3	River Confluence (STA 0+750)	15.80	15.46*	15.78*	15.93*	BACKWATER
4	Al-Jihad Mosque (STA 1+200)	16.55	16.09	16.38	16.43	SAFE

*Affected by sluice gate backwater (ΔH = 0.42-0.68 m).
Source: HEC-RAS simulation results, authors, 2025.

To distinguish the type of flood mechanism operating at each point, the controlling hydraulic indicator, either overflow margin or backwater step, was isolated and consolidated for direct comparison in Table 10.

Table 10. Controlling Indicator and Overflow/Backwater Margin at Q2

Point	Location	Controlling indicator	Margin at Q2	Mechanism type
1	Taman Husada Hospital	Overflow margin	+0.36 m	Compound area + low bank
2	Jalan Bandung	Overflow margin	+0.08 m	Pure bank overflow
3	River confluence	Backwater step	0.42-0.68 m	Undersized sluice gate
4	Al-Jihad Mosque	Freeboard	Positive (safe)	Latent constriction

Source: derived from Section 3.3 of this study.

Figure 5. Longitudinal Water Surface Profile of Bontang River (STA 0+000 to 1+936) for Q2, Q10, and Q20. Source: reconstructed from Table 9; linear interpolation between points, not the full 19 cross section HEC-RAS output.

At Point 1 (STA 0+125), the Q2 water surface elevation (15.23 m asl) exceeded the right bank crown (14.87 m asl) by 0.36 m, increasing to 0.78 m and 0.95 m under Q10 and Q20. The root cause is a compound deficiency of insufficient cross-sectional area combined with the critically low right bank, requiring full channel normalization. At Point 2 (STA 0+400), the Q2 water surface elevation (14.71 m asl) marginally exceeded the right bank crown (14.63 m asl) by 0.08 m, indicating pure bank overflow requiring right-bank levee raising rather than cross section enlargement.

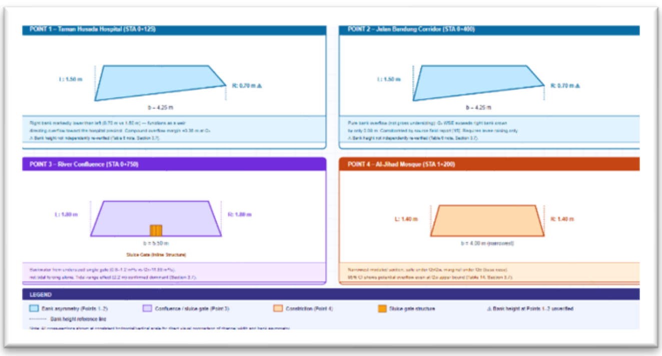

Figure 6. Schematic Cross Sectional Profiles at Observation Points 1-4. Bank height at Points 1-2 could not be independently re verified (Table 5 note, Section 2.2). Source: schematic trapezoidal reconstruction from Table 5 parameters; not a direct HEC-RAS geometry export.

At Point 3 (STA 0+750), the backwater originated from the single undersized sluice gate at the river confluence, not tidal forcing. The single operational gate accommodated only 0.8-1.2 m^3/s, a fraction of Q2 (11.88 m^3/s), independently confirmed using the submerged orifice equation (Eq. 3). At Point 4 (STA 1+200), channel width narrowed to 4.0 m, the narrowest modeled section. Under Q2 and Q10 the site remained hydraulically safe; under Q20 the freeboard margin narrowed to marginal status.

3.4 Model Validation

Because continuous streamflow gauging is unavailable, formal calibration in the Nash Sutcliffe or RMSE sense was not feasible. Model confidence rested on three independent lines of evidence: (1) overflow threshold consistency with field documented flood recurrence; (2) backwater consistency with field reported "water queuing" behavior; and (3) sensitivity robustness, with a WSE change of less than ±0.04 m at Point 1 under a ±0.005 Manning's n perturbation.

3.5 Flood Mitigation Simulation

Retention ponds are a widely adopted structural measure for attenuating peak urban flood discharge, with demonstrated effectiveness across a range of storm depths and catchment settings [29], [30]. A planned condition simulation was conducted for Q10 and Q20, incorporating two retention ponds, levee raising, and sluice gate augmentation from one to two openings.

Table 11. Retention Pond Design Parameters

Parameter	Pond 1 (Embung 1)	Pond 2 (Embung 2)
Peak inflow (design)	33.87 m^3/s	4.35 m^3/s
Allowable outflow	13.83 m^3/s	1.00 m^3/s
Peak attenuation	59.2%	77.0%
Required storage volume	31,122.27 m^3	7,191.93 m^3
Design depth	2.50 m	2.00 m
Required surface area	12,448.91 m^2	3,595.97 m^2
Available area	19,930.80 m^2	19,930.80 m^2
Land-feasibility status	Sufficient	Sufficient

Source: PENATEK 45 (2025) [22], hydrograph mass balance routing.

As an independent verification, mass-balance re-derivation using the Q20 hydrograph for Reach Bontang-1 alone (Table 3; Nakayasu parameters Tp=0.297 hr, T0.3=0.480 hr, sub-catchment area=1.29 km^2) against the allowable outflow of existing channel capacity (13.83 m^3/s, Table 6) yielded a storage requirement of 6,211 m^3 (2,484 m^2 at 2.50 m depth), approximately one-fifth of the original design value. This discrepancy indicates the original design inflow likely aggregates discharge contributions beyond the Reach Bontang 1 sub catchment; the precise delineation could not be independently re verified due to the unrecoverable geometry file (Section 2.2). This re-derivation is further propagated across the 95% confidence interval on Q20 in Table 14 (Section 3.7).

Table 12. Planned Condition Hydraulic Status: Existing vs. Planned Simulation

Observation point	Existing Q10	Planned Q10	Existing Q20	Planned Q20	Key intervention
Point 1 - RSUD Hospital	Flood	Safe	Flood	Safe	Retention Pond 1 + channel normalization
Point 2 - Jalan Bandung	Flood	Safe	Flood	Safe	Right-bank levee raising
Point 3 - River confluence	Backwater	Safe	Backwater	Safe	Sluice gate: 1 to 2 openings
Point 4 - Al-Jihad Mosque	Safe	Safe	Potential	Safe	Monitoring; pre-emptive normalization

Source: PENATEK 45 (2025) [22].

Note: Status categories reflect steady flow, normal depth boundary simulation only. The independent tidal-sensitivity check (Section 3.7, Table 15) shows the tidal range effect at Point 3 (approximately 2.2 m) substantially exceeds the sluice gate backwater step alone (0.42-0.68 m); the "Safe" status at planned condition Point 3 should be read as a gate-capacity based diagnostic finding, not a validated prediction under realistic tidal phasing.

The planned condition safety status at Point 3 should be treated as provisional pending coupled unsteady tidal hydraulic verification, rather than as a confirmed post-intervention outcome, given that the tidal range effect at this location is three to five times larger than the gate induced backwater step being addressed.

3.6 Discussion: Mechanism Interpretation

The nominal conveyance capacity of Reach Bontang 1 (13.83 m³/s) exceeds Q2 (11.88 m³/s), yet the channel floods below Q2. This apparent paradox resolves geometrically rather than volumetrically: the right bank stands only 0.70 m above the bed against a 1.50 m left bank, so the effective spill threshold is about 6.79 m³/s, well below full section capacity. This finding is consistent with, but extends beyond, prior single mechanism HEC-RAS studies [1], [3], [9], [12] by demonstrating that four hydraulically distinct mechanisms can co occur along a single short reach, each requiring a different targeted intervention rather than uniform treatment.

The transferable features of this case, a constrained structurally controlled outlet, asymmetric bank heights, and an undersized confluence gate, are common to many small coastal urban rivers in East Kalimantan and similar deltaic cities [31], [15], [16], [18], suggesting the diagnostic methodology, though not the specific numerical results, is portable to comparable settings.

3.7 Quantitative Bounding Checks: Discharge Uncertainty and Tidal Sensitivity

A formal 95% confidence interval on design discharge and its propagation to water surface elevation was computed using Kite's asymptotic method [27], providing a more rigorous basis than a simple linear discharge uncertainty extrapolation; results are presented in Table 13.

Table 13. 95% Confidence Interval on Design Discharge and WSE (Kite's Asymptotic Method)

T (years)	Q_T central (m³/s)	95% CI lower	95% CI upper
Q10	18.52	12.24	24.79
Q20	21.06	12.96	29.17

Point	Bank Elev. (m asl)	WSE Q10 CI [lower upper]	Overflow Q10 [lower upper]	WSE Q20 CI [lower upper]	Overflow Q20 [lower upper]
P1 (Hospital)	14.87	15.25-16.05	0.38-1.18 m	15.28-16.36	0.41-1.49 m
P2 (Jalan Bandung)	14.63	14.72-15.16	0.09-0.53 m	14.70-15.40	0.07-0.77 m
P4 (Al-Jihad Mosque)	16.55	16.11-16.65	Safe-0.10 m	16.27-16.59	Safe-0.04 m

Source: authors' calculation, 2026, Kite's asymptotic method applied to local rating curve (Table 9); 95% CI, t(0.975, df=9)=2.262.

Point 4, classified "Safe" at Q10 in the base simulation, shifts to marginal or actual overflow at the upper bound of the 95% confidence interval, indicating a materially greater overflow risk than the base case classification alone suggests, reinforcing the recommendation that explicit Q50/Q100 runs should precede final freeboard decisions.

Table 14. Propagation of Discharge Uncertainty to Pond 1 Storage Volume

Scenario	Q20 (m³/s)	Storage Volume	Area (2.50 m depth)	Land-Feasibility
Lower 95% CI bound	12.96	0 m³	0 m²	No storage needed
Central (base case)	21.06	6,211 m³	2,484 m²	Sufficient
Upper 95% CI bound	29.17	20,196 m³	8,078 m²	Sufficient
Original design [22]	33.87 (combined inflow)	31,122.27 m³	12,448.91 m²	Sufficient

Source: authors' calculation, 2026, mass balance routing applied to Table 13 discharge bounds.

At the upper bound (Q20=29.17 m³/s), required storage increased to 20,196 m³, more than three times the central estimate, reflecting significant sensitivity to discharge uncertainty from the short rainfall record. Even at this upper bound, the required area remained substantially below the available candidate land area (19,930.80 m²).

Table 15. Independent standard step backwater sensitivity at Point 3

Return period	WSE at Point 3, high tide (MHWS)	WSE at Point 3, low tide (MLWS)	ΔH (tidal-range effect)
Q10	17.91 m asl	15.69 m asl	2.22 m
Q20	18.15 m asl	15.91 m asl	2.24 m

Source: independent standard-step calculation, authors, 2026, n = 0.028, tidal datum from the national geospatial authority's tidal benchmark network.

The tidal range effect on WSE at Point 3 (approximately 2.2 m) was three to five times larger than the gate induced backwater step (0.42-0.68 m), indicating tidal stage is a material control on backwater magnitude at this location. This finding echoes broader evidence that tidal dynamics can dominate over structural discharge controls in compound coastal flood settings, where combined statistical hydrodynamic approaches and nonlinear tide surge interaction studies have similarly identified tidal forcing as a primary driver of peak water levels [32], [33].

The tidal datum (MHWS=+0.936 m, MLWS=-0.939 m) is referenced to national Mean Sea Level, whereas all elevations used elsewhere are referenced to the project's local Benchmark system. The elevation of the project's reference BM relative to national MSL was not available in the documentation reviewed, representing an unresolved datum reconciliation gap. However, the relative tidal range effect ($\Delta H \approx 2.2$ m) and its qualitative conclusion remain unaffected by a uniform datum shift, since both high and low tide simulations would shift equally. This independent check is offered as a bounding sensitivity analysis, not a substitute for coupled unsteady tidal hydraulic simulation.

4. CONCLUSION

This study applied one dimensional steady flow HEC-RAS 4.1 modeling to diagnose four hydraulically distinct flood mechanisms along a 1,936 m reach of the Bontang River: bank asymmetry overflow at Point 1, right bank levee overflow at Point 2, sluice gate backwater at Point 3, and a latent constriction at Point 4, each requiring a different intervention rather than uniform treatment. Two supplementary quantitative bounding checks sharpened this diagnosis: a formal 95% confidence interval discharge uncertainty projection showed Point 4 was more overflow prone than its base case status suggested, even at the upper bound of the 10 year discharge, and an independent standard step tidal check showed the tidal range effect at Point 3 (approximately 2.2 m) exceeded the gate induced backwater step alone. Planned condition simulation indicated that Points 1-3 shift to safe status under the 10 and 20 year design discharges in the base case scenario, though this result should be read alongside the discharge uncertainty and tidal sensitivity bounds before being treated as a final design basis.

These results address the research objectives stated in the Introduction: the four co occurring mechanisms were successfully diagnosed and differentiated, the channel capacity deficit was quantified, and mitigation performance was evaluated under uncertainty. The findings are indicative rather than definitive, given the absence of statistical calibration and the short 10 year rainfall record, though the bounding checks presented constrain this uncertainty quantitatively. Point 1 remains the highest mitigation priority given its proximity to a critical health facility, with Point 4 elevated to secondary near term priority based on the discharge uncertainty findings.

For future research, priority should be given to stream gauging for formal calibration, reconciliation of the project reference benchmark against the national geodetic datum, extension of the tidal bounding check toward a full unsteady simulation, and probabilistic discharge uncertainty quantification via numerical resampling methods [34], before the planned condition mitigation package is advanced to detailed structural design. Complementary nature-based interventions may also warrant consideration alongside the structural measures proposed here [35].

ACKNOWLEDGEMENT

The authors acknowledge the Bontang City Public Works and Spatial Planning Agency (PUPR) for funding the self-managed (swakelola) Bontang River flood control planning project from which the primary field data were obtained, and for granting permission to use these data for publication. The authors also acknowledge PENATEK 45, the Research and Community Service Center, Faculty of Engineering, Universitas 17 Agustus 1945 Samarinda, as the executing institution of the project, and its field survey team for conducting the topographic measurements and preparing the site plan drawings referenced in this article. The authors further acknowledge the Bontang City Dinas Pekerjaan Umum dan Penataan Ruang Kota and PT Ika Adya Perkasa Consulting Engineers & General Trading for the Bontang Urban Drainage System Master Plan referenced in Figure 3.

5. REFERENCES

[1] S. P. Sari, S. Suprayogi, and S. Budiman, "HEC-RAS-based urban flood simulation for enhancing mitigation scenarios in the Gajahwong River, Indonesia," *IOP Conf. Ser. Earth Environ. Sci.*, vol. 1453, no. 1, p. 12004, 2025, doi: 10.1088/1755-1315/1453/1/012004.

[2] M. Pangestu, R. R. R. Hadiani, and A. Y. Muttaqien, "Flood modelling of Premulung River, Bengawan Solo," *J. Appl. Agric. Sci. Technol.*, vol. 8, no. 1, pp. 1–14, 2024, doi: 10.55043/jaast.v8i1.183.

[3] K. Vashist and K. K. Singh, "HEC-RAS 2D modeling for flood inundation mapping: a case study of the Krishna River Basin," *Water Pract. Technol.*, vol. 18, no. 4, pp. 831–844, 2023, doi: 10.2166/wpt.2023.048.

[4] G. W. Brunner, *HEC-RAS River Analysis System: Hydraulic Reference Manual*, Version 6.3. Davis, CA, USA: US Army Corps of Engineers, Hydrologic Engineering Center, 2023.

[5] A. Negm and M. Elsahabi, "Review paper on applications of the HEC-RAS model for flooding, agriculture, and water quality simulation," *Water Pract. Technol.*, vol. 19, no. 7, pp. 2883–2901, 2024, doi: 10.2166/wpt.2024.183.

[6] N. K. Sari, N. Herlina, and H. Hidayanto, "Pemanfaatan model HEC-RAS dan metode ECLAC dalam menganalisis genangan banjir di Daerah Aliran Sungai Cilamajang," *Teras J. Tek. Sipil*, vol. 15, no. 1, pp. 100–113, 2025, doi: 10.29103/tj.v15i1.1207.

[7] S. Ali, M. Cheema, M. A. Bakhsh, and M. A. Waseem, "Flood inundation modeling by integrating HEC-RAS and satellite imagery: a case study of the Indus River Basin," *Water*, vol. 14, no. 19, p. 2984, 2022, doi: 10.3390/w14192984.

[8] S. A. Djafri, S. Cherhabil, M. A. Hafnaoui, and M. Madi, "Flood modeling using HEC-RAS 2D and IBER 2D: a comparative study," *Water Supply*, vol. 24, no. 9, pp. 3061–3076, 2024, doi: 10.2166/ws.2024.184.

[9] Y. Liu, M. Zhang, Z. Wang, and J. Li, "Improving flood inundation mapping accuracy using HEC-RAS modeling: a case study of the Neches River tidal floodplain in Texas," *J. Hydrol. Eng.*, vol. 29, no. 4, p. 5024009, 2024, doi: 10.1061/JHYEFF.HEENG-6037.

[10] A. Amiruddin, M. Roem, and R. Faizal, "Analisis tinggi muka air kanal bandara Kota Tarakan akibat pengaruh pasang surut menggunakan HEC-RAS 6.0," *Teras J. Tek. Sipil*, vol. 13, no. 2, pp. 301–312, 2023, doi: 10.29103/tj.v13i2.868.

[11] Y. A. Wibowo, A. Solichin, and R. R. R. Hadiani, "Risk-based zoning for urban flood mitigation using HEC-HMS-HEC-RAS 2D areas," *Adv. Sustain. Sci. Eng. Technol.*, vol. 8, no. 1, pp. 1–15, 2026, doi: 10.26877/asset.v8i1.2566.

[12] W. G. Bennett and others, "Modelling compound flooding: a case study from Jakarta, Indonesia," *Nat. Hazards*, vol. 118, no. 1, pp. 277–305, 2023, doi: 10.1007/s11069-023-06001-1.

[13] M. A. Budiyanto, M. Arifin, M. R. Iskandar, and I. Widyaningsih, "Open-access digital elevation model (DEM) selection for flood inundation modelling using HEC-RAS in Capital City of Nusantara," *IOP Conf. Ser. Earth Environ. Sci.*, vol. 1343, p. 12036, 2024, doi: 10.1088/1755-1315/1343/1/012036.

[14] K. Khatooni, F. Hooshyaripor, B. Malekmohammadi, and R. Noori, "A new approach for urban flood risk assessment using coupled SWMM-HEC-RAS-2D model," *J. Environ. Manage.*, vol. 374, p. 123849, 2025, doi: 10.1016/j.jenvman.2024.123849.

[15] P. Tiwari, A. D. Rao, and V. Pant, "Impact of land surface characteristics on coastal compound flooding using a coupled hydrodynamic-hydraulic modelling framework," *Sci. Rep.*, vol. 16, p. 15386, 2026, doi: 10.1038/s41598-026-46242-1.

[16] H. M. Benavides-Munoz and K. M. Roman-Aguilar, "Hydrodynamic modeling and flood mitigation strategies in an Andean valley city," *PLOS Water*, vol. 4, no. 7, p. e0000397, 2025, doi: 10.1371/journal.pwat.0000397.

[17] K. Nederhoff, R. Saleh, P. L. Barnard, and M. T. Stacey, "Mitigating flood risks in urban estuaries: tidal dynamics, shoreline hardening, nature-based solutions, and floodgates in San Francisco Bay," *J. Waterw. Port, Coastal, Ocean Eng.*, vol. 151, no. 6, p. 4025014, 2025, doi: 10.1061/JWPED5.WWENG-2342.

[18] S. Heo, W. Sohn, S. Park, and D. K. Lee, "Multi-hazard assessment for flood and landslide risk in Kalimantan and Sumatra: implications for Nusantara, Indonesia's new capital," *Heliyon*, vol. 10, no. 18, p. e37789, 2024, doi: 10.1016/j.heliyon.2024.e37789.

[19] M. B. Ansori, U. Lasminto, and A. A. G. Kartika, "Flood hydrograph analysis using synthetic unit hydrograph, HEC-HMS, and HEC-RAS 2D unsteady flow precipitation on-grid model for disaster risk mitigation," *Int. J. GEOMATE*, vol. 25, no. 107, pp. 50–58, 2023, doi: 10.21660/2023.107.3719.

[20] A. A. Yusuf, R. S. Ojo, M. O. Idrees, A. Balogun, I. B. Salami, and O. S. Sani, "Modelling flood hazards impacted by ungauged river in urbanised area using HEC-RAS and GIS," *Niger. J. Technol. Dev.*, vol. 20, no. 2, pp. 83–92, 2023, doi: 10.4314/njtd.v20i2.1405.

[21] J. Parthartlee and H. T. Puay, "Flow-dependent transport of glyphosate, dioxins, and lead in an urban river: a scenario-based HEC-RAS numerical study of Sungai Perai, Malaysia," *Int. J. Eng. Technol. Infrastruct. Dev.*, vol. 2, no. 2, pp. 250–258, 2026, doi: 10.3126/injet-indev.v2i2.95733.

[22] PENATEK 45, Universitas 17 Agustus 1945 Samarinda, "Laporan akhir: Kajian banjir di Kelurahan Gunung Telihan, Kota Bontang," Bontang, Indonesia, 2025.

[23] PENATEK 45, Universitas 17 Agustus 1945 Samarinda, "Survei dan Analisa Topografi (Bab IV, Laporan Akhir: Kajian Banjir di Kelurahan Gunung Telihan)," Bontang, Indonesia, 2025.

[24] A. H. Hussein and M. N. Kasim, "Utilizing statistical distribution tests to develop rainfall intensity-duration-frequency curves for enhanced hydrological analysis in Kirkuk city, Iraq," *Water Pract. Technol.*, vol. 19, no. 11, pp. 4378–4389, 2024, doi: 10.2166/wpt.2024.258.

[25] A. Aldrees and A. T. B. Taha, "Extreme daily rainfall assessment in arid environments through statistical modeling," *Atmosphere (Basel).*, vol. 17, no. 4, p. 402, 2026, doi: 10.3390/atmos17040402.

[26] Badan Standardisasi Nasional, "SNI 2415:2016 - Tata cara perhitungan debit banjir rencana," 2016, *BSN, Jakarta, Indonesia.*

[27] G. W. Kite, *Frequency and Risk Analyses in Hydrology*. Fort Collins, CO, USA: Water Resources Publications, 1977.

[28] World Meteorological Organization, *Guide to Hydrological Practices, Volume II*, 6th ed. Geneva, Switzerland: WMO, 2009.

[29] A. N. Pramono and P. T. Saputro, "Efektivitas kolam retensi terhadap pengendalian banjir," *G-SMART*, vol. 4, no. 2, pp. 75–84, 2021, doi: 10.24167/gsmart.v4i2.2331.

[30] E. Ahmadisharaf and others, "Effectiveness of retention ponds for sustainable urban flood mitigation across range of storm depths in Northern Tehran, Iran," *J. Sustain. Water Built Environ.*, vol. 7, no. 2, p. 4021004, 2021, doi: 10.1061/JSWBAY.0000946.

[31] S. Tsegaye, M. G. Kebedew, K. K. Albrecht, T. M. Missimer, S. Thomas, and A. S. Elshall, "Integrated GIS-hydrologic-hydraulic modeling to assess combined flood drivers in coastal regions: a case study of Bonita Bay, Florida," *Front. Water*, vol. 6, p. 1468354, 2024, doi: 10.3389/frwa.2024.1468354.

[32] H. Xu and others, "Combining statistical and hydrodynamic models to assess compound flood hazards from rainfall and storm surge: a case study of Shanghai," *Hydrol. Earth Syst. Sci.*, vol. 28, pp. 3919–3930, 2024, doi: 10.5194/hess-28-3919-2024.

[33] H. Du, K. Fei, and L. Gao, "Nonlinear tide-river-surge interactions and their impacts on compound flooding during Typhoon Hato in the Pearl River Delta," *J. Geophys. Res. Ocean.*, vol. 129, p. e2023JC020673, 2024, doi: 10.1029/2023JC020673.

[34] C. Shen and W.-B. Chen, "Projection of river discharge trends using machine learning and statistical uncertainty quantification," *J. Water Clim. Chang.*, vol. 17, no. 2, pp. 477–500, 2026, doi: 10.2166/wcc.2026.421.

[35] J. Griffiths, K. E. Borne, A. Semadeni-Davies, and C. C. Tanner, "Selection, planning, and modelling of nature-based solutions for flood mitigation," *Water*, vol. 16, no. 19, p. 2802, 2024, doi: 10.3390/w16192802.